Mechanics of Advanced Composite Structures 12 (2025), Serial Number 25, 435 – 446

Mechanics of Advanced Composite Structures

Journal homepage: https://macs.semnan.ac.ir/

Semnan University

ISSN: 2423-7043

Research Article - Part of the Special Issue on Mechanics of Advanced Fiber-Reinforced Composite Structures

Achieving High Strength in Fe-Based Metallic Glass Reinforced Aluminum Matrix Composites through Combined Ball Milling and Spark Plasma Sintering

Mohammad Reza Rezaei *, Reza Nazemnezhad, Erfan Khanmohammadi

School of Engineering, Damghan University, Damghan, 36716-45667, Iran

ARTICLE INFO

Article history:

Received: 2024-02-04

Revised: 2025-03-24

Accepted: 2025-04-16

Keywords:

Aluminum matrix composite;

Metallic glass particles;

Ball milling;

Spark plasma sintering;

Mechanical properties.

ABSTRACT

This study examines the production and analysis of aluminum matrix composites reinforced with Fe-based metallic glass (FMG) using powder metallurgy techniques. FMG particles with nominal composition Fe75Si15B5Zr5 were synthesized using the mechanical alloying process. For the fabrication of composites, two methods were used: (a) mixing gas atomized pure aluminum (GA) powder with FMG powder and consolidating via spark plasma sintering (SPS) to form the GA/FMG composite, and (b) ball milling the GA powder before mixing with FMG powder and SPS consolidation to produce the (GA+BM)/FMG composite. As a control, pure aluminum powders before and after the ball milling process were also consolidated using SPS under identical conditions, which were designated as GA and GA+BM, respectively. Results showed a notable difference in relative density (approximately 5%) between the (GA+BM)/FMG and GA/FMG composites. Quantitative analysis revealed that reinforcing particles were more evenly distributed in the GA/FMG composite. The (GA+BM)/FMG composite exhibited a compressive yield strength of 156 MPa, double that of the GA/FMG composite, but with reduced ductility. Fractography indicated that the (GA+BM)/FMG composite was more brittle than its GA/FMG counterpart.

1. Introduction

In recent years, there has been a growing demand for aluminum matrix composites with enhanced mechanical properties and reduced weight [1-4]. Incorporating various reinforcing particles, such as ceramic materials (e.g., SiC and Al2O3) and carbon-based materials (e.g., carbon nanotubes and graphene), into the aluminum matrix has significantly improved its strength and hardness [5-12]. However, due to differences in chemical composition and microstructure, the physical and chemical properties of the reinforcements, such as the coefficient of thermal expansion (CTE), differ from those of the metallic matrix [13]. As a result, the traditional reinforcements are often incompatible with the matrix, leading to weak interfacial bonding and the formation of micron-sized porosities, especially in the matrix/reinforcement interfacial region. This causes a significant decrease in the ductility and toughness of the composites [14, 15].

Metallic glasses have emerged as promising reinforcements to address these challenges [16-18]. Their exceptional mechanical properties, particularly high strength and toughness, make

* **Corresponding author.**
E-mail address: *m.r.rezaei@du.ac.ir*

Cite this article as:

Rezaei, M.R., Nazemnezhad, R. and Khanmohammadi, E., 2025. Achieving High Strength in Fe-Based Metallic Glass Reinforced Aluminum Matrix Composites through Combined Ball Milling and Spark Plasma Sintering. *Mechanics of Advanced Composite Structures*, 12(2), pp. 435-446.

https://doi.org/10.22075/MACS.2025.33187.1612

them well-suited for bolstering metallic materials [19, 20]. Two major methods have been used to produce metal matrix composites: solid-state methods and liquid-state methods [21, 22]. Powder metallurgy (PM) is a widely used solid-state method for synthesizing metallic glass-reinforced aluminum matrix composites [23-27].

Solid-state methods process metallic materials at lower temperatures than liquid-state techniques, avoiding phase changes between liquid and solid states. This approach allows for better control of the metastable structure of metallic glass reinforcements during composite synthesis. In powder metallurgy (PM), ball milling stands out as a widely used and economical technique. It effectively improves the distribution of reinforcements in metal matrix composites [28-30]. S. Sankaranarayanan et al.. [31] investigated the effect of ball milling on the microstructure and mechanical properties of Mg-(Ti + n-Al2O3) composites and found that ball milling positively influenced the distribution of reinforcing particles, resulting in enhanced strength and retention of ductility. Similarly, Salur et al. [32] successfully produced AA7075-Y2O3 nanocomposites via the PM method and reported that ball milling led to a remarkable increase in the hardness and strength of the composite.

After the preparation of solid powders, a consolidation process is required to produce bulk solids with full or near-full density. Several consolidation processes have been successfully used to achieve this goal, such as hot isostatic pressing (HIP) [33, 34], severe plastic deformation (SPD) [35, 36], and spark plasma sintering (SPS) [37-41]. SPS is a high-tech heating process that simultaneously applies direct heating and plastic deformation to the powders, resulting in the production of full or near-full dense bulk materials [42]. Several studies have investigated the microstructural and mechanical properties of metallic glass-reinforced composites produced by the SPS method. Guan et al.. [25] developed metallic glass-reinforced composites with core-shell structures by the surface crystallization of FMG particles via controlling the parameters of SPS and hot rolling. The results showed that the shell zone is effective in enhancing the mechanical properties of the composites. In another study by Kvashnin et al. [43], Fe-based metallic glass (FMG) particles reinforced 7075 aluminum matrix (Al-7075) composites that were prepared by the spark plasma sintering (SPS) technique. They found that adding FMG to Al alloy significantly improves the mechanical properties of consolidated samples.

While metallic glass-reinforced metal matrix composites have been widely studied, a comprehensive analysis of microstructural changes caused by combined ball milling and spark plasma sintering (SPS) processes in these materials is lacking. This study addresses this gap by combining ball milling and SPS techniques to produce an aluminum matrix composite reinforced with Fe-based metallic glass (FMG) particles. We examine the composite's microstructure, densification behavior, and mechanical properties.

2. Materials and Methods

2.1. Preparation of the Reinforcement Powder

Fe-based metallic glass (FMG) powder particles with a nominal composition (in at. %) of Fe75Si15B5Zr5 were produced using a high-energy planetary ball mill. A powder mixture of elemental Fe, Si, B, and Zr metals was ball milled in a wet medium (benzene). The ball-to-powder ratio was 16:1, the milling speed was 300 rpm, and the diameter of the balls was 10 mm. The milling of the mixture was continued for 30 hours [44].

2.2. Preparation of the Matrix Powder

Two types of powder particles were used for the matrix: (1) gas atomized high purity aluminum powder particles, and (2) the same gas atomized high purity aluminum powder particles that had been ball milled for 10 hours in a high-energy planetary ball mill using 1 wt% stearic acid as a process control agent (PCA). The ball-to-powder ratio of 8:1 and a milling speed of 300 rpm were selected for both types of powder particles.

2.3. Fabrication of the Composites

The synthesized FMG powder particles (10 vol. %) were mixed with the matrix powder particles (90 vol. %), which were prepared in gas atomized and gas atomized followed by ball milled conditions, using a low-energy horizontal jar mill. The reason for using low-energy milling was to restrict the detrimental reactions between the matrix powder particles and the amorphous reinforcing particles. The resulting composite powders were used to prepare bulk composite samples designated as GA/FMG and (GA+BM)/FMG, respectively. Monolithic gas-atomized pure Al powders, named GA, were used as reference material. Low-energy ball milling was performed at a milling speed of 100 rpm for 2 hours with a ball-to-powder ratio of 1:10.

To produce the bulk samples, the pure Al and reinforced Al composite powder particles were sintered using the SPS method. Figure 1 shows the DSC curve of Fe75Si15B5Zr5 (FMG) particles.

According to the curve, no chemical reaction occurred for FMG particles during heating to 580 °C (the glass transition temperature); hence, the sintering process should be performed below 580 °C. The powder particles were placed into a graphite die with an inner diameter of 25 mm and sintered for 10 minutes to reach a temperature of 550 °C. The heating rate and applied pressure were set to 50 °C/min and 40 MPa, respectively.

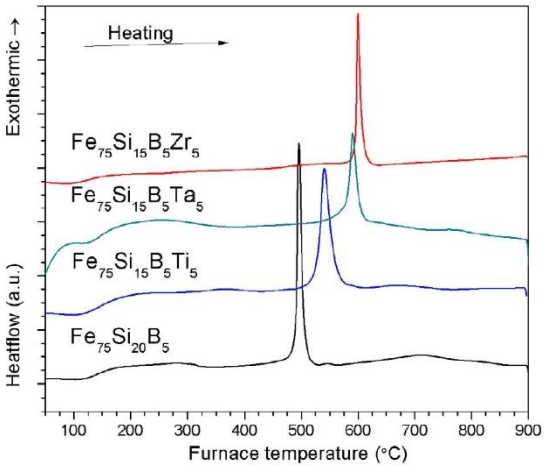

Fig. 1. DSC heating curves of amorphous $Fe_{75}Si_{15}B_5M_5$ (M = Si, Ti, Ta, Zr) powders obtained by wet milling [44].

2.4. Microstructure Observation and Mechanical Properties Tests

The bulk samples produced had a cylindrical shape with a diameter of 25 mm and a height of 20 mm. The density of the bulk samples was measured using Archimedes' method. This involved weighing the sample in air and then in distilled water using an electronic balance with an accuracy of ±0.0001 g. For degassing purposes, all the samples were boiled in distilled water for 40 minutes before weighing. The relative density of samples was calculated by dividing the measured density of each sample by its theoretical density. The microstructure and element distribution were analyzed using field emission scanning electron microscopy (FESEM, ZEISS Sigma 300) and energy-dispersive spectroscopy (EDS). The software ImageJ was used to quantify the microstructural features of powder and bulk samples.

To analyze the phase of the samples, X-ray diffraction (XRD) was carried out using a diffractometer with Cu Kα radiation for a scan range of 20°-90°. To calculate the stored dislocation density from the XRD patterns, the Williamson-Hall equation was employed [45, 46]:

$$B \cos\theta = \frac{K\lambda}{D} + 4\varepsilon \sin\theta \quad (1)$$

where B is the full width at half maximum (FWHM) of a peak, θ is the diffraction angle, K is a constant, and λ is the wavelength of the X-ray. The term $B \cos\theta$ was plotted along the Y-axis and $4 \sin\theta$ along the X-axis to construct the Williamson–Hall plots. Then, a straight line was fitted to the data points; its slope and y-intercept provided the microstrain (ε) and crystalline size (D), respectively. From the calculated lattice microstrain and crystallite size, the stored dislocation density was determined by using the following equation [47]:

$$\rho = \frac{2\sqrt{3}\varepsilon}{Db} \quad (2)$$

where ρ is the dislocation density and b is the Burgers vector.

The standard compression test samples were machined with a height-to-diameter ratio of 1.5 from the bulk samples. Hardness tests were carried out in the Brinell scale with an indenter of 2.5 mm and a load of 31.25 kg. The uniaxial compression test was performed using a Santam apparatus according to ASTM E9, with a strain rate of 1.0× 10-3 s-1 maintained. The tests were continued until the onset of fracture. Each sample was tested 4 times, and took the average value was used to decrease the error.

3. Results and Discussion

3.1. Characterization of the Powders

Figure 2 displays FESEM micrographs and related particle size distribution histograms of the synthesized FMG powder particles (i.e., the reinforcing particles) as well as the matrix powder particles before and after ball milling. As shown in Figure 2(a), the FMG powders are equiaxed and possess an irregular surface with an average size of 7 µm. Figure 2(b) illustrates the atomized pure Al powders, which are uniform in size and semi-spherical in appearance, with a smooth surface and an average particle size of 19 µm. Figure 2(c) presents the pure Al powders after ball milling, which exhibit facetted morphology and have an average particle size of 38 µm. This morphology is caused by the shear action of the balls. During further milling, particles start to fracture, leading to the creation of irregularly shaped particles having smaller sizes [48].

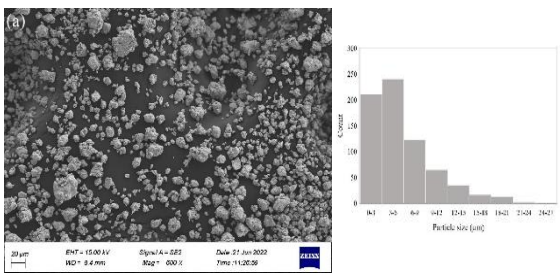

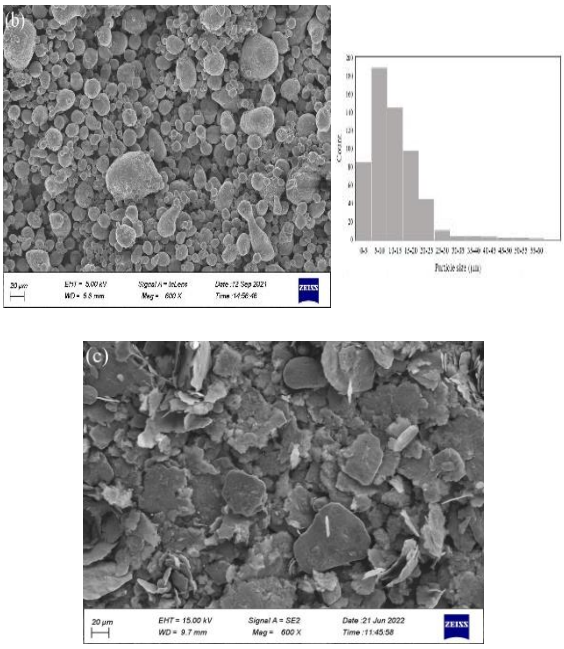

Fig. 2. FESEM micrographs and related particle size distribution: (a) metallic glass particles, (b) GA powder, FESEM micrographs, (c) GA+BM powder

Figure 3 illustrates the XRD patterns obtained from FMG powders as well as GA powders before and after the ball milling process. According to Fig. 3(a), a diffuse hump was observed around 2θ=44° which indicates the amorphous structure of the synthesized FMG particles. As expected, Figure 3(b) shows sharp crystalline peaks that correspond to pure Al. However, after ball milling, some peak broadening, as well as a significant reduction in intensity, can be observed. These changes may be attributed to the impact force of milling media on the pure Al particles, which leads to lattice strain and the creation of microstructural defects such as dislocations. The lattice strain (ε) can be quantitatively calculated using the Williamson-Hall method.

The results indicate that the lattice strain of pure Al powders significantly increased from 5×10^{-5} to 7×10^{-4} after the ball milling process.

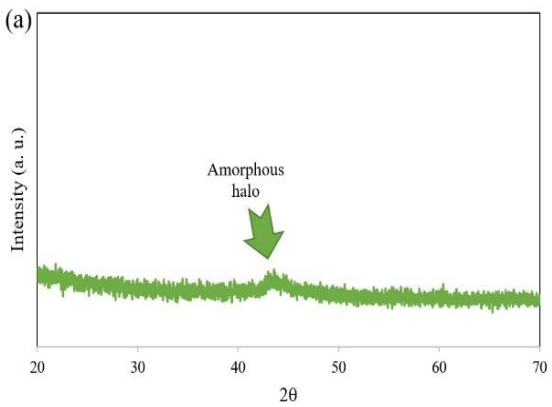

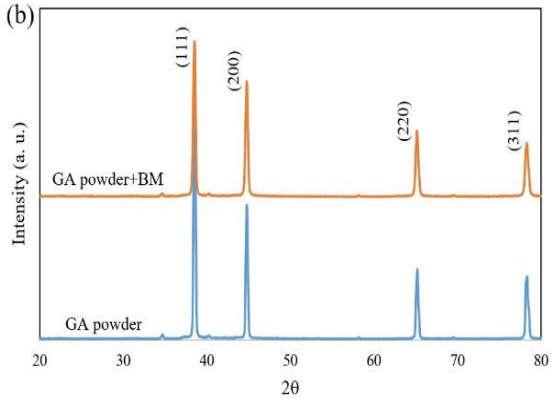

Fig. 3. XRD patterns: (a) synthesized FMG powder, (b) GA powder before and after BM process

3.2. Characterization of the Consolidated Samples

Figure 4 shows the density measurement results from this study. As expected, the GA sample achieved near full density after sintering. But, for GA+BM, the relative density decreased to approximately 0.94. As discussed in section 3.1, the ball milling process induces severe plastic deformation in pure Al powders, leading to more lattice strain and dislocations, and thus significantly increasing the powder's hardness. This, in turn, reduces the followability of pure Al particles, making microscopic pores more likely to form under imposed pressure during the sintering process. Adding FMG particles to the gas-atomized matrix (GA/FMG) and ball-milled matrix ((GA+BM)/FMG) had minimal impact on their relative density. This is due to the metallic nature of FMG particles, which makes them compatible with matrix powder particles and reduces the likelihood of pore formation in the matrix/reinforcement interface.

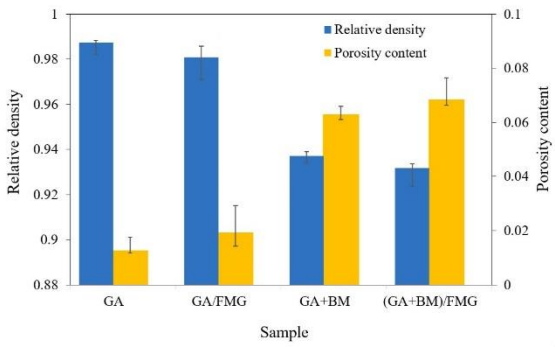

Fig. 4. Relative densities of sintered samples

Figure 5 displays the FESEM micrographs and corresponding EDS maps of sintered composite samples. The metallic glass reinforcements are visible in both micrographs as white areas, as confirmed by the EDS mapping images of the element Fe, which is the main constituent element of FMG particles. The distribution of

reinforcing particles in the matrix is a critical parameter that affects the behavior of composite materials. As shown in Fig. 5, the distribution of FMG particles is more homogeneous in the GA/FMG composite than in the (GA+BM)/FMG composite.

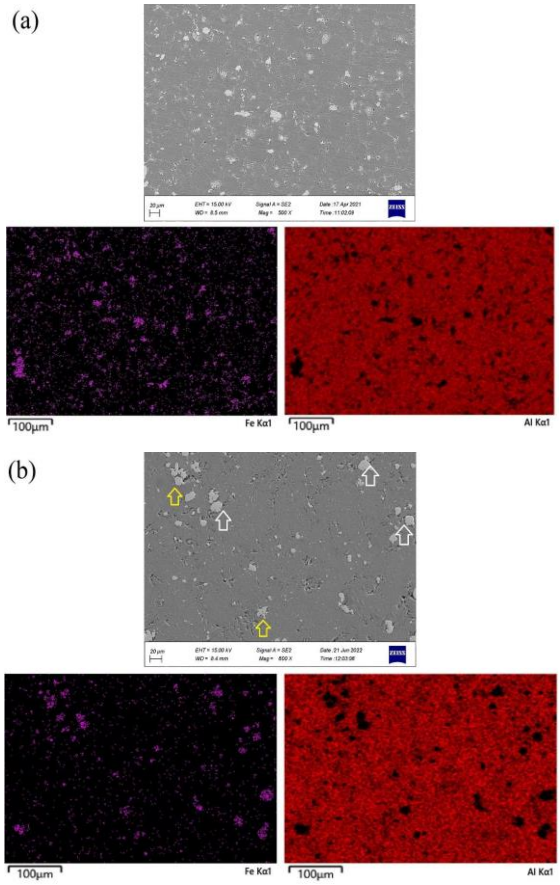

Fig. 5. FESEM micrographs and EDS maps: (a) GA/FMG, (b) (GA+BM)/FMG. FMG clusters (yellow arrows), interfacial porosities (white arrows)

The quadrat method, a reliable statistical approach, helps quantify the spatial distribution of reinforcing particles [49, 50]. In this method, the image is divided into square cells (quadrats) of a size approximately twice the mean area per particle [51]. The number of particles per quadrant, Nq, is counted. For this study, quadrats with sides of 25 µm were considered based on the average size of FMG particles. Each micrograph was divided into 192 quadrants, and three images of each sample were analyzed. The results are shown in Fig. 6, where a more symmetric Nq distribution (closer frequency of empty quadrats and quadrats containing more than three particles) indicates a more homogeneous distribution of reinforcing particles [49]. The GA/FMG composite shows a much more homogeneous distribution of FMG particles in the matrix compared to the (GA+BM)/FMG composite, consistent with microstructural observations. This can be attributed to the lower hardness of GA powder particles before ball milling, allowing the matrix powder particles in GA/FMG composite to flow more easily between FMG particles during the sintering process and resulting in a more homogeneous distribution of FMG particles in the matrix.

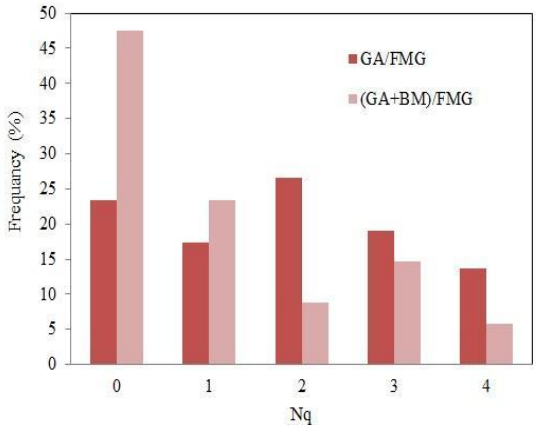

Fig. 6. Reinforcing particle distribution in the matrix of samples

The formation of clean interfaces, devoid of any micro-pores or other discontinuities, between the matrix and FMG reinforcements in the GA/FMG composite, is evidenced by observations made in Fig. 5(a). This phenomenon can be attributed to the compatibility of the FMG reinforcements, which contain metallic elements, with the matrix. However, Fig. 5(b) shows some discontinuities (dark spots) in the matrix/reinforcement interface of the (GA+BM)/FMG composite. This may be due to the increased hardness of the matrix materials after ball milling, which could have reduced the compressibility and accommodation of both the matrix and reinforcement particles.

Also, according to Fig. 7, which shows the distribution of elements in the Al/FMG region, no interfacial chemical products formed between the reinforcements and the matrix. This can be related to the short sintering time, which is one of the important features of the SPS process [52].

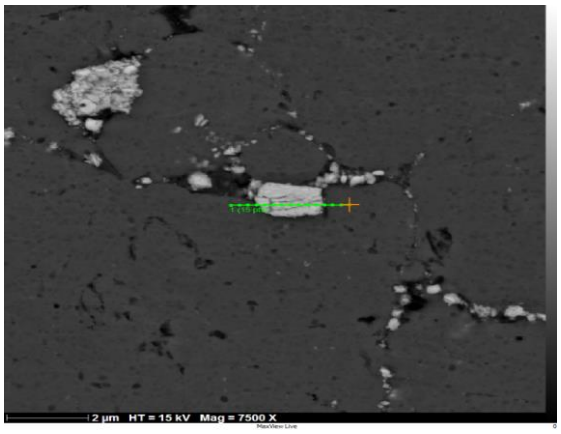

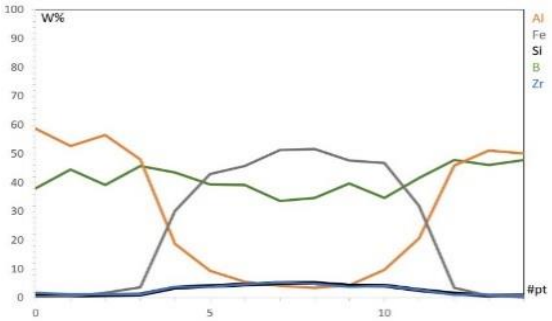

Fig. 7. FESEM micrographs and EDS line analysis within the matrix/reinforcements interfacial region of (GA+BM)/FMG

Figure 8 illustrates the XRD patterns of the sintered samples. Once again, the crystalline peaks of Al, serving as the matrix material, are observed in all samples. Additionally, the (GA+BM)/FMG composite exhibits lower intensity and greater broadening of crystalline peaks when compared to the other samples. A comparison between the patterns in Figs. 8 and 3 reveal that the sintering process does not impact the characteristics of the crystalline peaks. Given the short holding time (about 5 minutes) at peak temperature during sintering, mass transport is limited to a few microns. As a result, the interior structure of the particles remains unaltered, allowing for most of the stored lattice strain to be preserved in the sintered samples. Furthermore, Fig. 8(b) indicates the presence of an amorphous halo at the 2θ angle of ~44° adjacent to the Al (200) peak. This suggests the stability of the metastable structure of the metallic glass reinforcements during the sintering process.

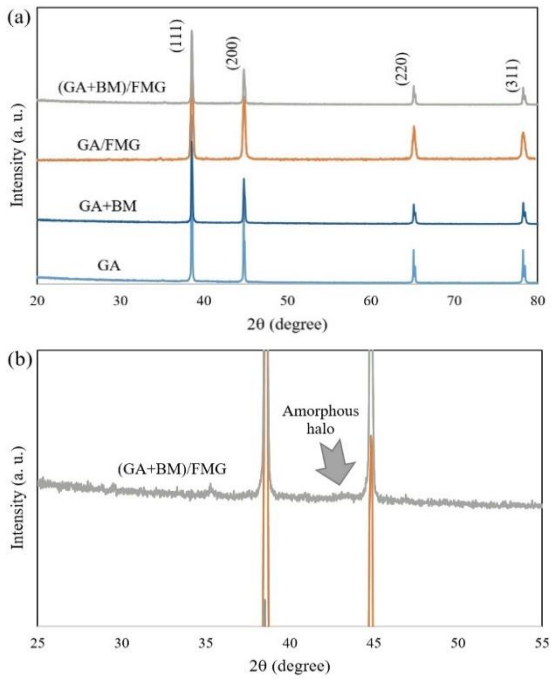

Fig. 8. XRD patterns: (a) different samples, (b) enlarged pattern of (GA+BM)/FMG

Figure 9 shows the values for the dislocation density of the different samples. These values were determined using the Williamson-Hall method. The figure reveals a substantial increase in the dislocation density of the ball-milled samples (GA+BM and (GA+BM)/FMG)) compared to the GA and GA/FMG samples. These alterations can be attributed to the intense plastic deformations experienced during the ball milling process. Also, the difference in the coefficient of thermal expansion (CTE) between FMG particle and aluminum matrix leads to the formation of dislocations in the matrix of composite samples (GA/FMG and (GA+BM)/FMG)) upon cooling from the sintering temperature.

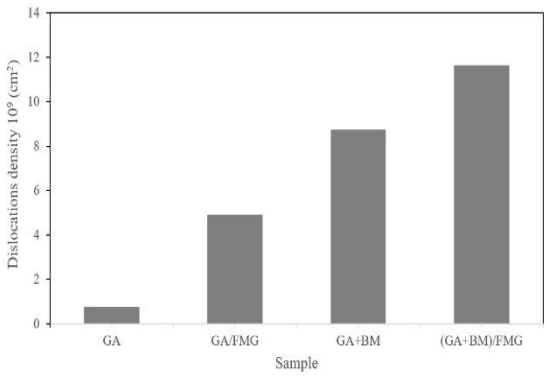

Fig. 9. Dislocation density values for various samples.

3.3. Mechanical Properties of the Consolidated Samples

Figure 10 shows the results of the Brinell hardness measurements for different samples. The results indicate that the hardness of the (GA+BM)/FMG composite is about 63.5 BHN, which is significantly higher than the GA/FMG composite (39.7 BHN).

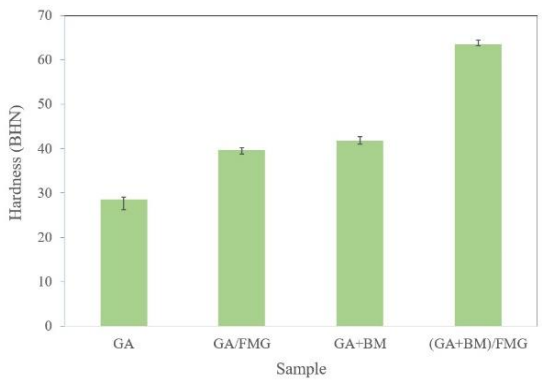

Fig. 10. Hardness values of different samples

Figure 11 and Table 1 display the outcomes of the compression tests. The compressive properties of some previously developed Al matrix composites consolidated through SPS are also given in the table. The compressive yield strength of the sintered pure Al sample (GA) is

considerably enhanced upon the addition of metallic glass particles to the matrix (GA/FMG). This increase in strength and hardness has a minor impact on compressive ductility, as has been previously reported for metallic glass-reinforced composites [53]. The metallic nature of metallic glass materials boosts the composite's strength and forms a strong reinforcement/matrix interface. This interface helps counteract the negative effects often seen in ceramic-reinforced composites, where cracks typically start during loading. It's important to note that FMG particle size influences the composite's strength and ductility. Generally, micron-sized reinforcements increase composite strength but reduce ductility [31, 54]. Thus, the minor reduction in ductility can be attributed to the size of the FMG particles. Moreover, the role of reinforcing particle morphology in the mechanical properties should not be ignored. The sharp edges of particles typically cause stress concentration near them during loading [55]. Therefore, the relatively rounded edges of FMG particles (Fig. 4) could be another reason for the exceptional ductility observed in the GA/FMG composite.

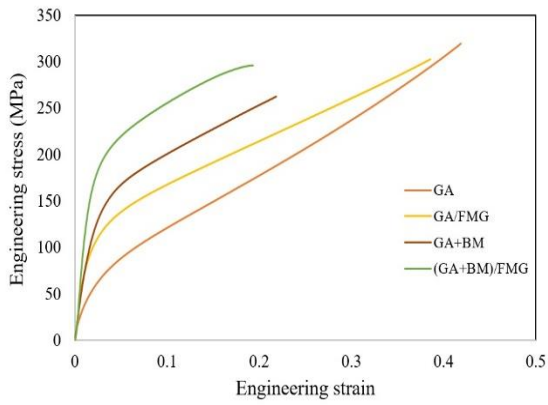

Fig. 11. Compression stress-strain curves for different samples.

Table 1. Compressive mechanical properties of samples

Sample	Fabrication method	0.2% Yield strength (MPa)	Hardness (BHN)	Strain to fracture	Ref.
GA	SPS	48±3	28	0.42±0.04	This work
GA/FMG	SPS	85±4	39	0.38±0.02	This work
GA+BM	BM+SPS	112±4	42	0.23±0.01	This work
(GA+BM)/FMG	BM+SPS	156±7	63	0.19±0.02	This work
Al/$Al_{65}Cu_{20}Ti_{15}$ metallic glass	SPS	-	29	-	[56]
6061 aluminum alloy/AlCoCrFeNi high-entropy alloy	SPS	94	-	0.12	[57]
Al/FMG/SiC hybrid reinforced	SPS	98		0.62	[42]

Additionally, the (GA+BM)/FMG composite exhibited a significant increase of approximately 83% in compressive yield strength when compared to the GA/FMG composite. However, this increase in strength was accompanied by a remarkable reduction in ductility, which decreased by approximately 50%. It is important to note that the high-energy ball milling process was performed only on the matrix material before adding the reinforcing particles, so its effects on the mechanical properties should be considered only in terms of the matrix. Moreover, the influence of the matrix's condition on the distribution of reinforcing particles and the matrix/reinforcement interfacial region should not be overlooked. Also, a comparison of the mechanical properties of samples developed in the current work with previously developed composites (Table 1) shows that the combination of ball milling and SPS processes results in better mechanical properties compared to SPS alone.

The contribution of effective strengthening mechanisms in enhancing the yield strengths of the samples can be calculated through the following equation:

$$\sigma_y = \sigma_0 + \Delta\sigma_G + \Delta\sigma_{Dis} + \Delta\sigma_{Load} \quad (3)$$

where σ_0 is the friction stress (~20 MPa), and $\Delta\sigma_G$, $\Delta\sigma_{dis}$, and $\Delta\sigma_{Load}$ are the increases in the yield strength caused by grain refinement, dislocation, and load-bearing of reinforcements, respectively.

$\Delta\sigma_{dis}$ can be estimated by the following equation [58]:

$$\Delta\sigma_{Dis} = M\alpha Gb\sqrt{\rho} \quad (4)$$

where α is constant equal to 0.24 and ρ is the dislocation density stored in the lattice, which is illustrated in Fig. 9.

The contribution of the load-bearing strengthening mechanism in the enhancement of yield strength can be calculated using [59]:

$$\Delta\sigma_{Load} = \frac{1}{2} V_P \sigma_M \tag{5}$$

where V_P is the volume fraction of FMG particles and σ_M represents the yield strength of the matrix.

Based on the total yield strength of different samples (Table 1) and knowing the contribution of dislocation and load-bearing of reinforcements mechanisms, and according to equation (3), the contribution of grain refinement mechanism can be determined. Figure 12 shows the contribution of the above-mentioned mechanisms to the overall yield strengths of the different samples.

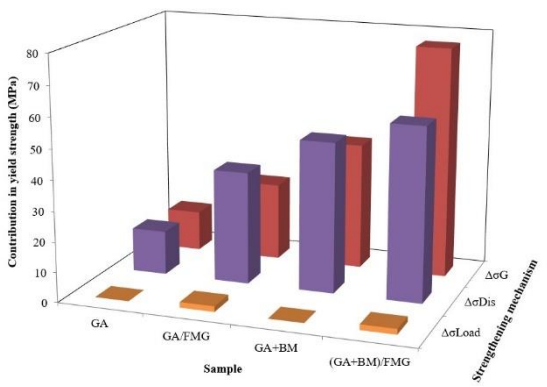

Fig. 12. The contributions of the strengthening mechanisms to the yield strengths of the samples

According to Figure 12, the contribution of dislocation and grain refinement mechanisms in the strengthening of material is more pronounced in ball-milled samples (GA+BM and (GA+BM)/FMG). The high-energy ball milling process imposed lattice strain on the pure Al powder used for producing GA+BM and (GA+BM)/FMG samples, which shows itself as dislocations in the microstructure. Hence, these two strengthening mechanisms can be considered responsible for the higher strength of ball-milled samples. However, the ball milling process negatively influences the ductility of consolidated samples in two ways: first, the distribution of reinforcing particles, and second, matrix/reinforcements interfacial characteristics. As previously discussed in Section 3.2, the ball milling process negatively affected the distribution of reinforcing particles in the matrix material during the SPS process. The non-homogeneous distribution of reinforcements in the matrix results in decreasing the distance between matrix/reinforcement interfaces. Therefore, under external loading, the propagation of cracks originating from the interfaces and linking them up with other cracks would be promoted, resulting in decreased ductility of the consolidated composite. Additionally, microscopic pores were created in the matrix/reinforcement interfacial regions of the (GA+BM)/FMG composite, as seen in Fig. 5. The presence of micropores negatively affected the strength of interface bonds and acted as crack initiation sites. Thus, the ductility of the (GA+BM)/FMG composite could be decreased again due to the propagation of interfacial cracks.

3.4. Fracture Behavior

Figure 13 shows the compressive fracture surfaces of the composite samples. Both samples exhibit shear bands, a common feature of their fracture surfaces. The distortion of the composites under compression loading leads to the formation of shear bands. As a result of uneven straining of distinct microstructural zones during compressive loading, more shear bands are visible in the GA/FMG composite, which has a softer aluminum matrix and hard reinforcements, than in the (GA+BM)/FMG composite.

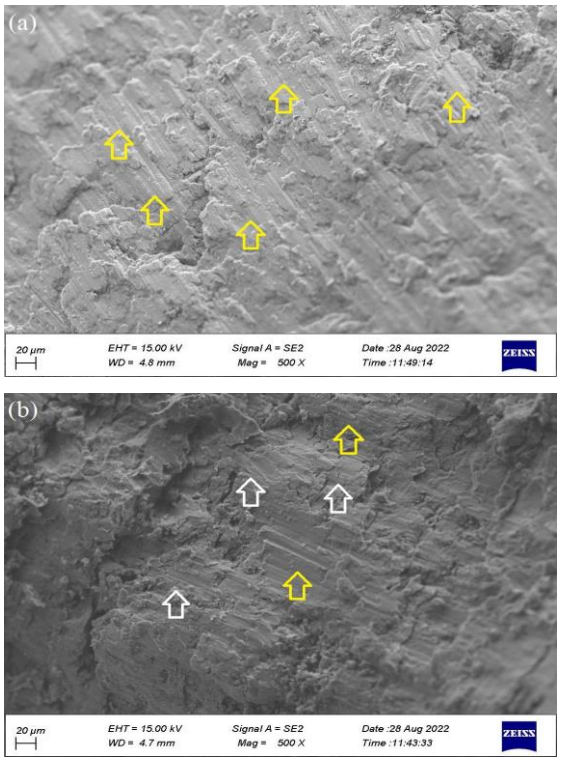

Fig. 13. Fracture surfaces: (a) GA/FMG, (b) (GA+BM)/FMG. Shear bands (yellow arrows), micro-cracks (white arrows)

In contrast, Fig. 13(b) shows that the fracture surface of the (GA+BM)/FMG composite features micro-cracks that stem from segregated reinforcing particles, confirming the rationale

presented in section 3.3 for the reduced ductility of this composite relative to the GA/FMG composite. As loading continues, these micro-cracks grow into larger cracks [60], visible in Fig. 13(b), eventually leading to the composite's failure.

4. Conclusions

This study yielded several key findings:

1) FMG-reinforced Al matrix composites were successfully produced using gas-atomized matrix powder (GA/FMG) and gas-atomized then ball-milled matrix powder ((GA+BM)/FMG).
2) The best densification behavior occurred for the GA/FMG composite.
3) During sintering, micron-sized pores formed in the matrix/reinforcement interfaces of the (GA+BM)/FMG composite.
4) The (GA+BM)/FMG composite showed markedly improved compressive yield strength (about 83% higher than the GA/FMG composite), but its ductility was limited due to the uneven distribution of FMG particles and high porosity.
5) The predominant methods for the improvement of (GA+BM)/FMG strength were the grain refinement and dislocation strengthening mechanisms.
6) Both (GA+BM)/FMG and GA/FMG composites displayed distortion-induced shear bands on their fracture surfaces. However, only the (GA+BM)/FMG composite showed micro-cracks."

Funding Statement

This research did not receive any specific grant from funding agencies in the public, commercial, or not-for-profit sectors.

Conflicts of interest

The author declares that there is no conflict of interest regarding the publication of this article.

References

[1] He, Y., Xu, H., Liu, Y., Chen, Y. & Ji, Z., 2022. Strengthening mechanism of b4c@ apc/al matrix composites reinforced with bimodal-sized particles prepared by hydrothermal carbonized deposition on chips. *Journal of Materials Science & Technology, 123*, pp.60-69.

[2] Guo, B., Song, M., Zhang, X., Cen, X., Li, W., Chen, B. & Wang, Q., 2020. Achieving high combination of strength and ductility of al matrix composite via in-situ formed ti-al3ti core-shell particle. *Materials Characterization, 170*, pp.110666.

[3] Han, Y., Liu, J., Wang, Q., Lin, C., Wang, E., Wu, W. & Zhang, M., 2022. Effect of volume fraction ratio of ti to al3ti on mechanical and tribological performances of the in situ ti–al3ti core–shell structured particle reinforced al matrix composite. *Journal of Materials Research, 37*(21), pp.3695-3707.

[4] Ghods, H., Manafi, S. & Borhani, E., 2015. Effect of particle size on the structural and mechanical properties of al–aln nanocomposites fabricated by mechanical alloying. *Mechanics Of Advanced Composite Structures, 2*(2), pp.73-78.

[5] Liu, W., Ke, Y., Sugio, K., Liu, X., Guo, Y. & Sasaki, G., 2022. Microstructure and mechanical properties of al2o3-particle-reinforced al-matrix composite sheets produced by accumulative roll bonding (arb). *Materials Science and Engineering: A, 850*, pp.143574.

[6] Hu, J., Zhang, J., Luo, G., Sun, Y., Shen, Q. & Zhang, L., 2021. Effectively enhanced strength by interfacial reactions in in-situ carbon reinforced al matrix composites. *Vacuum, 188,* pp.110148.

[7] Han, T., Wang, F., Li, J., Zhao, N. & He, C., 2021. Simultaneously enhanced strength and ductility of al matrix composites through the introduction of intragranular nano-sized graphene nanoplates. *Composites Part B: Engineering, 212,* pp.108700.

[8] Zhang, X. & Chen, T., 2021. Simultaneously enhancing the strength and ductility of particulate-reinforced aluminum matrix composite by aging treatment. *Journal of Materials Research, 36*(17), pp.3445-3459.

[9] Altunpak, Y. & Akbulut, H., 2017. Mechanical properties of a squeeze-cast 2124 al composite reinforced with alumina short fibre. *Metallurgical Research & Technology, 114*(5), pp.509.

[10] Azadi, M. & Kamali, F., 2020. A comparative study on the microstructure and mechanical properties of al-si-cu/1wt% ncp composites after t6 heat treatment. *Mechanics Of Advanced Composite Structures, 7*(1), pp.129-136.

[11] Hsieh, C.-T., Ho, Y.-C., Wang, H., Sugiyama, S. & Yanagimoto, J., 2020. Mechanical and tribological characterization of

nanostructured graphene sheets/a6061 composites fabricated by induction sintering and hot extrusion. *Materials Science and Engineering: A, 786*, pp.138998.

[12] Şenel, M.C. & Mahmutoğlu, Ü., 2022. Effect of induction heat treatment on the mechanical properties of si3n4–graphene-reinforced al2024 hybrid composites. *Bulletin of Materials Science, 45*(1), pp.48.

[13] Guan, H.D., Li, C.J., Peng, Y.Z., Gao, P., Feng, Z.X., Liu, Y.C., Li, J.N., Tao, J.M. & Yi, J.H., 2022. Fe-based metallic glass particles carry carbon nanotubes to reinforce al matrix composites. *Materials Characterization, 189*, pp.112006.

[14] Rezaei, M., Albooyeh, A., Chachei, R. & Malahi, P., 2022. Effect of the spark plasma sintering temperature on the microstructure and mechanical properties of a ceramic/metallic glass reinforced hybrid composite. *Journal of Composite Materials, 56*(17), pp.2779-2788.

[15] Jayalakshmi, S. & Gupta, M., 2015. *Metallic amorphous alloy reinforcements in light metal matrices*. Springer.

[16] Wang, Z., Xie, M.S., Zhang, W.W., Yang, C., Xie, G.Q. & Louzguine-Luzgin, D.V., 2020. Achieving super-high strength in an aluminum based composite by reinforcing metallic glassy flakes. *Materials Letters, 262*, pp.127059.

[17] Khan, A., Reddy, M.M., Reddy Matli, P., Shakoor, R.A. & Gupta, M., 2021. *Development and properties of amorphous particles reinforced al matrix nanocomposites*. *In:* BRABAZON, D. (ed.) *Encyclopedia of materials: Composites.* Oxford: Elsevier, pp.96-108.

[18] Rezaei, M., Shabestari, S. & Razavi, S., 2019. Investigation on equal-channel angular pressing-induced grain refinement in an aluminum matrix composite reinforced with al-cu-ti metallic glass particles. *Journal of Materials Engineering and Performance, 28*(5), pp.3031-3040.

[19] Gupta, P., Majumdar, B., Katakareddi, G. & Yedla, N., 2021. Cu50zr50 metallic glass flakes reinforced al composites: Experimental and molecular dynamics nanoindentation response of matrix, interface, and reinforcement. *Journal of Non-Crystalline Solids, 564*, pp.120837.

[20] He, T., Lu, T., Ciftci, N., Uhlenwinkel, V., Chen, W., Nielsch, K. & Scudino, S., 2020. Interfacial characteristics and mechanical asymmetry in al2024 matrix composites containing fe-based metallic glass particles. *Materials Science and Engineering: A, 793*, pp.139971.

[21] Xie, X., Yin, S., Raoelison, R.-N., Chen, C., Verdy, C., Li, W., Ji, G., Ren, Z. & Liao, H., 2021. Al matrix composites fabricated by solid-state cold spray deposition: A critical review. *Journal of Materials Science & Technology, 86*, pp.20-55.

[22] Yadav, M., Kumaraswamidhas, L.A. & Singh, S.K., 2022. Investigation of solid particle erosion behavior of al-al2o3 and al-zro2 metal matrix composites fabricated through powder metallurgy technique. *Tribology International, 172*, pp.107636.

[23] Zheng, R., Yang, H., Liu, T., Ameyama, K. & Ma, C., 2014. Microstructure and mechanical properties of aluminum alloy matrix composites reinforced with fe-based metallic glass particles. *Materials & Design, 53*, pp.512-518.

[24] Wang, Z., Tan, J., Scudino, S., Sun, B., Qu, R., He, J., Prashanth, K., Zhang, W., Li, Y. & Eckert, J., 2014. Mechanical behavior of al-based matrix composites reinforced with mg58cu28. 5gd11ag2. 5 metallic glasses. *Advanced Powder Technology, 25*(2), pp.635-639.

[25] Guan, H.D., Li, C.J., Gao, P., Yi, J.H., Bao, R., Tao, J.M., Fang, D. & Feng, Z.X., 2020. Fe-based metallic glass particles reinforced al-7075 matrix composites prepared by spark plasma sintering. *Advanced Powder Technology, 31*(8), pp.3500-3506.

[26] Yu, P., Kim, K.B., Das, J., Baier, F., Xu, W. & Eckert, J., 2006. Fabrication and mechanical properties of ni–nb metallic glass particle-reinforced al-based metal matrix composite. *Scripta Materialia, 54*(8), pp.1445-1450.

[27] Rezaei, M.R., Shabestari, S.G. & Razavi, S.H., 2018. Effect of ecap consolidation process on the interfacial characteristics of al-cu-ti metallic glass reinforced aluminum matrix composite. *Composite Interfaces, 25*(8), pp.669-679.

[28] Chen, Y., Hu, Z., Xu, Y., Wang, J., Schützendübe, P., Huang, Y., Liu, Y. & Wang, Z., 2019. Microstructure evolution and interface structure of al-40 wt% si composites produced by high-energy ball milling. *Journal of Materials Science & Technology, 35*(4), pp.512-519.

[29] Doğan, K., Özgün, M.İ., Sübütay, H., Salur, E., Eker, Y., Kuntoğlu, M., Aslan, A., Gupta, M.K. & Acarer, M., 2022. Dispersion mechanism-induced variations in microstructural and mechanical behavior of cnt-reinforced

aluminum nanocomposites. *Archives of Civil and Mechanical Engineering, 22*(1), pp.55.

[30] Hong, J., Zou, J., Chen, W., Jiang, C., Yuan, H., Huang, F., Liu, W. & Zhang, X., 2023. Effect of ball milling time on the microstructure and properties of cu(al)-tic0.5 composites. *Journal of Materials Engineering and Performance, 32(13)*, pp.5956-5966.

[31] Sankaranarayanan, S., Jayalakshmi, S. & Gupta, M., 2011. Effect of ball milling the hybrid reinforcements on the microstructure and mechanical properties of mg–(ti+ n-al2o3) composites. *Journal of alloys and compounds, 509*(26), pp.7229-7237.

[32] Salur, E., Aslan, A., Kuntoğlu, M. & Acarer, M., 2021. Effect of ball milling time on the structural characteristics and mechanical properties of nano-sized y2o3 particle reinforced aluminum matrix composites produced by powder metallurgy route. *Advanced Powder Technology, 32*(10), pp.3826-3844.

[33] Zhu, W., Liu, W., Ma, Y., Cai, Q., Wang, J. & Duan, Y., 2021. Microstructural characteristics, mechanical properties and interfacial formation mechanism of tungsten alloy/steel composite structure fabricated by hip co-sintering. *Materials & Design, 211*, pp.110127.

[34] Chen, H., Mi, G., Li, P. & Cao, C., 2022. Excellent high-temperature strength and ductility of graphene oxide reinforced high-temperature titanium alloy matrix composite fabricated by hot isostatic pressing and heat treatment. *Composites Communications, 30*, pp.101077.

[35] Edalati, K., Ashida, M., Horita, Z., Matsui, T. & Kato, H., 2014. Wear resistance and tribological features of pure aluminum and al–al2o3 composites consolidated by high-pressure torsion. *Wear, 310*(1), pp.83-89.

[36] Korznikova, G., Czeppe, T., Khalikova, G., Gunderov, D., Korznikova, E., Litynska-Dobrzynska, L. & Szlezynger, M., 2020. Microstructure and mechanical properties of cu-graphene composites produced by two high pressure torsion procedures. *Materials Characterization, 161*, pp.110122.

[37] Nie, Q., Chen, G., Wang, B., Yang, L., Zhang, J. & Tang, W., 2022. Effect of invar particle size on microstructures and properties of the cu/invar bi-metal matrix composites fabricated by sps. *Journal of Alloys and Compounds, 891*, pp.162055.

[38] Souza, R.M., Ordoñez, M.F.C., Mezghani, S., Crequy, S., Fukumasu, N.K., Machado, I.F. & El Mansori, M., 2020. Orthogonal cut of sps-sintered composites with ferrous matrix and femos particles: Numerical and experimental analysis. *Tribology International, 149*, pp.105750.

[39] Liu, R., Wang, W., Chen, H., Tan, M. & Zhang, Y., 2018. Microstructure evolution and mechanical properties of micro-/nano-bimodal size b4c particles reinforced aluminum matrix composites prepared by sps followed by her. *Vacuum, 151*, pp.39-50.

[40] Mohammadtaheri, M., Bozorg, M., Yazdani, A. & Salehi, M., 2022. Fabrication of ti–al2o3–ha composites by spark plasma sintering and its properties for medical applications. *Journal of Materials Research, 37*(16), pp.2571-2580.

[41] Zeng, W., Qin, W., Gu, C., Sun, H., Ma, Y. & Cao, X., 2019. Microstructure and properties of pure aluminum prepared by spark plasma sintering. *Metallurgical Research & Technology, 116(3)*, pp.312.

[42] Rezaei, M., Albooyeh, A., Shayestefar, M. & Shiraghaei, H., 2020. Microstructural and mechanical properties of a novel al-based hybrid composite reinforced with metallic glass and ceramic particles. *Materials Science and Engineering: A, 786*, pp.139440.

[43] Kvashnin, V.I., Gerasimov, E.Y., Novoselov, A.N., Legan, M.A., Lukyanov, Y.L., Bataev, I.A., Emurlaev, K.I., Bokhonov, B.B. & Dudina, D.V., 2024. Structural characteristics and mechanical properties of partially reacted and non-reacted al–fe66cr10nb5b19 metallic glass composites. *Vacuum, 224*, pp.113201.

[44] Neamțu, B., Chicinaş, H., Marinca, T., Isnard, O., Chicinaş, I. & Popa, F., 2016. Synthesis of amorphous fe75si20− xmxb5 (m= ti, ta, zr) via wet mechanical alloying and its structural, thermal and magnetic characterisation. *Advanced Powder Technology, 27*(2), pp.461-470.

[45] Williamson, G. & Hall, W., 1953. X-ray line broadening from filed aluminium and wolfram. *Acta metallurgica, 1*(1), pp.22-31.

[46] Warren, B. 1969. X-ray diffraction, courier corporation. Reading, MA, Addison-Wesley Publishing Company.

[47] Zhao, Y., Liao, X., Jin, Z., Valiev, R. & Zhu, Y.T., 2004. Microstructures and mechanical properties of ultrafine grained 7075 al alloy processed by ecap and their evolutions during annealing. *Acta Materialia, 52*(15), pp.4589-4599.

[48] Sadeghi, B., Cavaliere, P. & Castro, M.M., 2024. Optimizing ball milling parameters for controlling the internal microstructure and tensile characteristics of a laminated carbon nanotube/aluminum-copper-magnesium composite. *Journal of Alloys and Compounds, 984*, pp.173927.

[49] Tzamtzis, S., Barekar, N., Babu, N.H., Patel, J., Dhindaw, B. & Fan, Z., 2009. Processing of advanced al/sic particulate metal matrix composites under intensive shearing–a novel rheo-process. *Composites Part A: Applied Science and Manufacturing, 40*(2), pp.144-151.

[50] Haslam, M.D. & Raeymaekers, B., 2013. A composite index to quantify dispersion of carbon nanotubes in polymer-based composite materials. *Composites Part B: Engineering, 55*, pp.16-21.

[51] Curtis, J.T. & Mcintosh, R.P., 1950. The interrelations of certain analytic and synthetic phytosociological characters. *Ecology, 31*(3), pp.434-455.

[52] Rezaei, M., Nazemnezhad, R. & Farahmandrad, S., 2023. Effects of the si element on the microstructure and mechanical properties of an al/fmg/sic hybrid composite. *Materials Chemistry and Physics, 309*, pp.128343.

[53] Ertugrul, O., He, T., Shahid, R.N. & Scudino, S., 2019. Effect of heat treatment on microstructure and mechanical properties of al 2024 matrix composites reinforced with ni60nb40 metallic glass particles. *Journal of Alloys and Compounds, 808*, pp.151732.

[54] Xie, M.S., Wang, Z., Zhang, G.Q., Yang, C., Zhang, W.W. & Prashanth, K.G., 2020. Microstructure and mechanical property of bimodal-size metallic glass particle-reinforced al alloy matrix composites. *Journal of Alloys and Compounds, 814*, pp.152317.

[55] Qin, S., Chen, C., Zhang, G., Wang, W. & Wang, Z., 1999. The effect of particle shape on ductility of sicp reinforced 6061 al matrix composites. *Materials Science and Engineering: A, 272*(2), pp.363-370.

[56] Abolkassem, S., Elsayed, A., Kariya, S., Umeda, J. & Kondoh, K., 2023. Influence of thermo-mechanical processing on microstructure and properties of bulk metallic glassy alloys-reinforced al matrix composites prepared by powder metallurgy. *Journal of Materials Research and Technology, 27*, pp.8197-8208.

[57] An, X., Li, F., Kan, L., Zhang, W., Wang, J., Jin, X., Wang, Y., Li, J., Zhu, H., Qi, W., Wei, W. & Sun, W., 2025. High entropy alloy particle reinforced 6061 aluminum matrix composites: An investigation of mechanical strength and thermoelectric properties. *Journal of Alloys and Compounds, 1010*, pp.177424.

[58] Sarkar, A., Bhowmik, A. & Suwas, S., 2009. Microstructural characterization of ultrafine-grain interstitial-free steel by x-ray diffraction line profile analysis. *Applied Physics A, 94*, pp.943-948.

[59] Miller, W. & Humphreys, F., 1991. Strengthening mechanisms in particulate metal matrix composites. *Scripta metallurgica et materialia, 25* (1), pp.33-38.

[60] Guan, L., Cao, H., Su, Y., Zhang, D., Liu, K., Hua, A., Peng, Y., Zhao, H. & Ouyang, Q., 2024. Enhanced strength–ductility synergy of sic particles reinforced aluminum matrix composite via dual configuration design of reinforcement and matrix. *Materials & Design, 245*, pp.113186.